Research Article

Revati Radakisnin, Mohd Shukry Abdul Majid*, Mohd Ridzuan Mohd Jamir, Mohd Faizal Mat Tahir, Cheng Ee Meng, and Hassan Al Alshahrani

Physical, thermal, and mechanical properties of highly porous polylactic acid/cellulose nanofibre scaffolds prepared by salt leaching technique

https://doi.org/10.1515/ntrev-2021-0098
received July 17, 2021; accepted September 24, 2021

Abstract: This study aimed to prepare and characterise polylactic acid (PLA) reinforced with cellulose nanofibre (CNF) from a *Pennisetum purpureum*-based composite scaffold and determine its structural and mechanical properties. Porous scaffolds with CNF compositions of 5–20 wt% in the PLA matrix were developed using solvent casting and particulate leaching of its porogen at 90 wt% of loadings. Morphology studies using field emission scanning electron microscopy revealed that the scaffolds had well-interconnected pores with an average pore size range of 67–137 µm and porosity >76%. X-ray diffraction confirmed the interconnectivity and homogeneity of the pores and the fibrous structure of the scaffolds. The compressive strength of the fabricated scaffolds varied between 2.34 and 6.66 MPa, while their compressive modulus was between 1.95 and 6.04 MPa for various CNF contents.

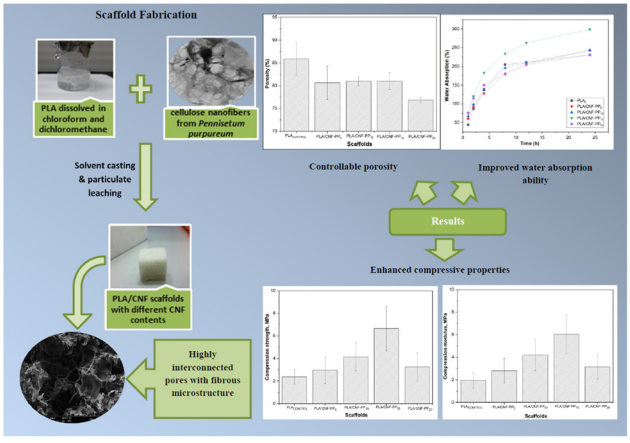

Graphical abstract

Furthermore, water absorption and thermal degradation studies showed that the scaffold had good hydrophilicity and improved thermal stability. These findings highlight the need to modify the pore structure and mechanical performance simultaneously for tissue engineering. Thus, this study concludes that the developed PLA scaffolds reinforced with CNF from *Pennisetum purpureum* are potential candidates for cell attachment and extracellular matrix generation.

Keywords: highly porous polylactic acid, *Pennisetum purpureum*, cellulose nanofibres-reinforced scaffold, mechanical properties, salt leaching technique

Abbreviations

CNF	cellulose nanofibre
CNF-PP	cellulose nanofibres from *Pennisetum purpureum*
DTG	derivative thermogravimetry
ECM	extracellular matrix
FESEM	field emission scanning electron microscopy
FTIR	Fourier transform infrared

* **Corresponding author: Mohd Shukry Abdul Majid,** Faculty of Mechanical Engineering Technology, Universiti Malaysia Perlis (UniMAP), Pauh Putra Campus, Arau 02600, Perlis, Malaysia, e-mail: shukry@unimap.edu.my
Revati Radakisnin: Faculty of Mechanical Engineering Technology, Universiti Malaysia Perlis (UniMAP), Pauh Putra Campus, Arau 02600, Perlis, Malaysia; Faculty of Electronic Engineering Technology, Universiti Malaysia Perlis (UniMAP), Pauh Putra Campus, Arau 02600, Perlis, Malaysia
Mohd Ridzuan Mohd Jamir: Faculty of Mechanical Engineering Technology, Universiti Malaysia Perlis (UniMAP), Pauh Putra Campus, Arau 02600, Perlis, Malaysia
Mohd Faizal Mat Tahir: Center for Integrated Design of Advanced Mechanical Systems (PRISMA), Faculty of Engineering and Built Environment, Universiti Kebangsaan Malaysia, Bandar Baru Bangi 43600, Selangor, Malaysia
Cheng Ee Meng: Faculty of Electronic Engineering Technology, Universiti Malaysia Perlis (UniMAP), Pauh Putra Campus, Arau 02600, Perlis, Malaysia
Hassan Al Alshahrani: Department of Mechanical Engineering, Najran University, King AbdulAziz Road, PO Box 1988, Najran, Saudi Arabia

PLA	polylactic acid
TGA	thermogravimetric analysis
XRD	X-ray diffraction

1 Introduction

Soft tissue is comprised of a variety of tissues, including skin, fat, tendons, muscles, nerves, articular cartilage, blood vessels, and fascia. Its role in the human body includes supporting, surrounding, and combining the body structure and internal organs [1]. Autologous implantation has been traditionally used to repair and regenerate damaged or diseased tissues and organs. Due to complications associated with autologous transplantations, such as rapid loss in volume and easily absorb approximately 40–60% of soft tissue cells, remain feasible, as reported by Yuksel *et al.* [2]. The constraints associated with existing treatments have led researchers to develop new biological replacements to overcome the limitations of current clinical treatments by exploring alternative biomaterials, such as polymeric scaffolds incorporated with nanocellulose.

With the development and emergence of nanotechnology, cellulose, the most abundant material on earth, revitalised and gained significant attention as a novel and leading material in the form of nanocellulose [3]. Nanocellulose is a unique and vital natural material extracted from cellulose (found in bacteria, animals, and plants) in the form of nanostructures. Typically, nanocellulose can be classified as cellulose nanofibres (CNFs), cellulose nanocrystals, and bacterial cellulose [4–6]. Generally, CNFs can be obtained from plants, especially from bast fibres or wood, by chemical or mechanical treatment [7]. Therefore, CNF is a promising biomaterial that has been highly recommended for use in tissue engineering and regenerative medicine as a reinforcement of polymeric scaffolds for cell culture. The most common features when outlining the importance of CNFs are their high specific surface area, hydrophilicity, renewability, adjustable morphological and mechanical reinforcements, biocompatibility, biodegradability, and non-toxicity, as mentioned by Hickey and Pelling [8]. Associated with tissue engineering and regenerative medicine topics, these factors facilitate polymeric scaffolds with reinforced CNF with enhanced properties, such as high mechanical strength, surface modifications, and biological properties.

Pennisetum purpureum, commonly known as Napier grass, comprises cellulose, hemicellulose, and lignin in the proportions of 46, 34, and 20%, respectively [9]. It grows rapidly and requires minimal nutrient supplementation. CNFs from *Pennisetum purpureum* were chosen for this study because they are an abundant and sustainable resource found across many Asian countries [10]. Recent studies have confirmed the use of *Pennisetum purpureum* fibres as a suitable reinforcement [11]. Reddy *et al.* studied the structural and chemical composition of Napier grass fibres and found morphological differences between the treated and untreated fibres, with improved tensile properties identified in the former [9]. Subsequently, Ridzuan *et al.* explored the potential of *Pennisetum purpureum* as reinforcement for polymer composites. They found that alkaline treatment increased the surface roughness and improved the tensile stress of the fibres [12]. A further study by De Araújo Morandim-Giannetti *et al.* evaluated the effect of delignification conditions on Napier grass and proved the suitability of Napier grass as a source for composites with low degradation under optimal conditions for the industrial processes of bleaching and pulping [13]. Many studies have highly recommended the use of CNFs as fillers in polymeric scaffolds [14,15]. Radakisnin *et al.* synthesised CNFs from *Pennisetum purpureum* using ball milling assisted by acid hydrolysis treatment [16]. They found that chemical and mechanical treatments had a minimal effect on its cellulosic properties; as a result, the thermal stability and the effective surface area available for contact were enhanced. More recently, researchers have begun to study the benefits of nanocomposites in biomedical applications [17], providing evidence for using CNFs from *Pennisetum purpureum* as reinforcement in polymeric scaffolds.

In tissue engineering, polylactic acid (PLA) has been approved by the Food and Drug Administration for use in the controlled release of drugs and biodegradable polymers [14,15]. As PLA is the most common and medically approved material, it has been widely used to produce scaffolds, as well as due to its superior biodegradability and biocompatibility [18]. Dai *et al.* mentioned that PLA is widely used in the field of tissue-engineered repair, and it decomposed into pyruvate and glycolate and hydrolysed into water (H_2O) and carbon dioxide (CO_2) eventually *in vivo* [19]. It can also be degraded into lactic acid, where the degradation time of PLA can be altered *via* copolymerisation [17,20,21]. In addition, this polymer is non-toxic and is removed by the body using the normal metabolic system [22]. Recently, several researchers have developed PLA scaffolds as preliminary support platforms in tissue engineering [18,23]. However, PLA scaffolds exhibit poor mechanical performance and hydrophobicity. Donate *et al.* regarded that PLA exhibits low osteoconductivity, inadequate cell adhesion on its surface, and intrinsic acidic degradation [24].

Therefore, PLA reinforced with CNFs from *Pennisetum purpureum* is viewed as highly favourable as a biocomposite

in tissue engineering [14,25]. If both materials can be incorporated, CNFs will be able to neutralise the acidic degradation produced by PLA. Furthermore, the reinforcement of CNFs could improve the mechanical properties, especially its microstructure, to facilitate the bioactivity of the scaffolds [26]. According to Peng *et al.*, solvent casting and particulate leaching is a traditional construction method used to fabricate scaffolds with a macroporous structure for soft tissue engineering [27]. However, effectively blending PLA with CNFs using solvent casting and particulate leaching remains a challenge due to the behaviour of CNFs, which tend to agglomerate. Ultrasonication is a reliable mechanical method to disperse CNFs in liquids where they increase the dispersion by breaking the agglomerations in aqueous suspensions. However, the efficiency is highly dependent on the applied force of the probe reported by Chanda and Bajwa [28]. Hence, ultrasonication can be used during the fabrication process to resolve this and produce scaffolds with well-dispersed CNF particles.

This study evaluates the performance of PLA scaffolds reinforced with various CNFs from *Pennisetum purpureum* using solvent casting and particulate leaching techniques. The porosity and microstructural properties of the scaffolds were evaluated under fixed environmental conditions, and the pore size of each scaffold was measured using ImageJ. The compressive strength and modulus were measured using a cantilever stress–strain tester machine to analyse the influence of compressive strength, modulus, CNF composition, and the contribution of porogens to the scaffolds. Based on these findings, PLA scaffolds with various CNFs from *Pennisetum purpureum* were formulated, and their properties, including water absorption, structural morphologies, and thermal properties, were determined.

2 Materials and methods

2.1 Materials

CNFs from *Pennisetum purpureum* (Napier fibres) were developed using Napier grass supplied from a local plantation (Bukit Kayu Hitam, Kedah, in northern peninsular Malaysia). Dichloromethane (DCM), chloroform, and ethanol were obtained from Thermo Fisher Scientific (Waltham, MA, USA). Analytical grade sodium chloride (NaCl) was purchased from Merck (Darmstadt, Germany) and was used as a porogen. Medical grade PLA (M_W 60,000) used to fabricate scaffolds was acquired from Sigma-Aldrich (Missouri, United States).

2.2 Preparation of PLA/CNFs composite

Porous PLA/CNFs from *Pennisetum purpureum* (CNF-PP) scaffolds were fabricated using solvent casting and particulate leaching. First, PLA pellets with known weight were dissolved in an organic solvent to achieve a viscous solution of 1.2 g/20 mL. The ratio of chloroform to DCM was kept constant at 1:1. Next, the PLA solution was stirred using a magnetic stirrer and heated at 70°C for 30 min. Then, CNFs from *Pennisetum purpureum* were dispersed in the PLA solution. To uniformly disperse CNF-PP in the PLA solution, the mixture was ultrasonicated for 10 min at 40% amplitude to eliminate any CNF-PP agglomerates. As a result, the contents of CNF-PP were selected as 0, 5, 10, 15, and 20 wt%, as illustrated in Table 1. Subsequently, the addition of porogen to the PLA/CNF-PP solution was blended at a ratio of 9:1. Thus, prior to mixing the porogen-PLA/CNF-PP mixture and stirring for 2 h, the PLA/CNF-PP mixture was ready for casting. Subsequently, the cast scaffold was oven-dried overnight at 40°C. Next, the prepared scaffolds were immersed in deionised water for three days to leach out the salt (porogen) and form the composite scaffolds, which were refreshed every 8 h to remove the salt residual entirely. Subsequently, oven drying was carried out for the salt-leached scaffolds at room temperature for two days, and the resultant PLA/CNF-PP scaffolds were prepared. Details on the structural, morphological, and thermal properties of CNFs from *Pennisetum purpureum* (CNF-PP) are described in detail in a previous study [16].

Table 1: Composition, porosity, and average pore size of CNFs-reinforced PLA-based scaffolds

Scaffold samples	CNF content (wt%)	Porogen content (%)	Porosity (%)	Average pore size (μm)
PLA_C	0	90	85.87	134.00 ± 40.18
PLA/CNF-PP_5	5	90	80.63	136.68 ± 67.31
PLA/CNF-PP_{10}	10	90	80.98	102.98 ± 41.63
PLA/CNF-PP_{15}	15	90	81.01	81.48 ± 24.23
PLA/CNF-PP_{20}	20	90	76.89	67.58 ± 18.96

2.3 Morphological study using field emission scanning electron microscopy (FESEM)

The morphological analysis of the PLA scaffolds reinforced with various CNFs from *Pennisetum purpureum* was characterised by FESEM (Zeiss Merlin; Jena, Germany) at an accelerating voltage of 20 kV. Each specimen was cut to an approximate dimension of 10 mm × 10 mm. The samples were mounted on aluminium stubs and subsequently sputter-coated with gold to avoid unwanted charges and to enhance conductivity. The surface morphology, pore size, and interconnectivity of the pores of the scaffolds were also evaluated in this testing. The pore sizes of each scaffold were further measured from the FESEM images using ImageJ software.

2.4 Porosity measurements

As mentioned by Lopes *et al.* [22] and Massai *et al.* [29], in the generally adopted theoretical model, the microstructure of a porous scaffold can be obtained internally by dividing the pore space into a collection of single pores, where it can be defined as parts of the void space limited by solid surfaces. Thus, the porosity of the scaffold can be described as a void fraction of the scaffolds.

The porosity of the scaffolds was evaluated using the ethanol displacement technique. Archimedes' principle of buoyancy was used for the porosity tests. Absolute ethanol was used as a liquid displacement as it easily penetrated the pores and did not induce shrinkage or swelling as a non-solvent of the scaffold composite. The initial weight of dry scaffolds, W_1, was measured and then the dry scaffold was immersed in ethanol with a known weight, $W_{\text{ethanol,}}$ in a specimen bottle. A series of low-pressurisation cycles above the ethanol saturation pressure were conducted to force ethanol into the pores [30]. The process was repeated until no air bubbles were observed on the surface of the specimens. Subsequently, the total weight of the ethanol and ethanol-impregnated scaffold was recorded as W_2. The samples were then kept in ethanol for 2 h. The ethanol-impregnated scaffold was removed, and the residual ethanol weight was recorded as W_3. The void volume of the scaffold is calculated as follows:

$$V_{\text{VOID}} = \frac{W_2 - 2W_1 - W_3}{\rho_{\text{ethanol}}}. \quad (1)$$

The total volume of the scaffold was calculated as:

$$V_{\text{TOTAL}} = \frac{W_2 - W_1 - W_3}{\rho_{\text{ethanol}}}. \quad (2)$$

The accessible porosity was determined as the ratio of the volume of the void scaffold to the total volume of the scaffold, as follows:

$$\text{Porosity (\%)} = 100 \times \frac{W_2 - 2W_1 - W_3}{W_2 - W_1 - W_3}. \quad (3)$$

2.5 X-ray diffraction (XRD) analysis

XRD was performed to determine the crystalline systems present in each scaffold using a D2 phase Bruker diffractometer with Cu-Kα radiation (λ = 1.5418 Å) at 30 mA and 40 kV. The diffraction pattern of the scaffolds was scanned in the range of $10° < 2\theta < 80°$ at a scan rate of 4°/min and a step size of 0.02° in continuous mode. The crystallinity index (CrI) was estimated using the peak height method, as shown in equation (4):

$$\text{CrI (\%)} = 100 \times \frac{I_{200} - I_{\text{am}}}{I_{200}}, \quad (4)$$

where I_{200} and I_{am} represent the intensities of the crystalline and amorphous regions of the scaffolds, respectively.

2.6 Fourier transform infrared (FTIR) analysis

Infrared spectra were used to identify the functional groups present in the scaffolds. The scaffolds were analysed using FTIR spectroscopy (RX1; Perkin-Elmer, UK). The ground precipitate of the scaffolds was mixed with KBr. The absorption spectra were recorded in the range of 400–4,000 cm^{-1} with a resolution of 1 cm^{-1}.

2.7 Thermogravimetric analysis (TGA)

The thermal stability of PLA scaffolds with different compositions of CNFs from *Pennisetum purpureum* was evaluated using a TG analyser and derivative thermogravimetry (DTG 60H; Shimadzu, Japan). Scaffolds weighing 10 mg were mounted on an alumina crucible and evaluated over a temperature range of 30–800°C under a nitrogen atmosphere at a heating rate of 20°C/min.

2.8 Water absorption measurements

The water absorption measurements were evaluated using a simplified method. The specimens were cut with a

dimension of 10 mm × 10 mm × 10 mm, dried to a constant weight, W_{DRY}, and then immersed and soaked in distilled water at room temperature of 25°C for the required time (1, 2, 4, 8, 12, and 24 h). The soaked specimens were then removed from the distilled water and weighed, and the excess water on the surface of the specimens was gently blotted with a filter paper to obtain W_{WET}. The percentage of water absorption for the specimens at various times was calculated as follows:

$$\text{Water absorption (\%)} = 100 \times \frac{W_{WET} - W_{DRY}}{W_{DRY}}, \quad (5)$$

where W_{DRY} and W_{WET} are the weights of the dried scaffolds and wet scaffolds at the required times, respectively [31]. For each scaffold, four specimens were tested, and the mean values were recorded.

2.9 Mechanical analysis

The compression strength and modulus properties of the scaffolds were determined to evaluate the effect of CNF-PP addition on the mechanical properties of the PLA scaffolds. Testing was performed according to ASTM D695-96 [32] standard using an Autograph AG-X Plus Universal Tensile Tester machine (Shimadzu). The specimens were cut into rectangular sections (13 mm thickness × 25 mm length × 13 mm width). The test was carried out at a cross-head speed of 1.0 mm/min using a 10 kN load cell. In order to obtain flat surfaces, the top and bottom layers of the scaffolds were detached. The dimensions of the specimens were measured manually before testing using a Vernier calliper. The compression strength of the scaffolds was determined as the stress at which the samples were compressed to 30% of their original thickness. The compression modulus was measured from the slope of the stress–strain curve. Five samples were evaluated for each scaffold, and the average values were recorded.

3 Results and discussion

3.1 Morphology and porosity study of scaffolds

For biocompatibility in tissue engineering, a scaffold should have an ideal pore size, porosity, high interconnectivity, and good cytotoxicity to enhance cell attachment and proliferation [33]. In the present study, CNFs from *Pennisetum purpureum* as a reinforcement filler to control pore size and porosity to promote good cytocompatibility, were introduced. Figure 1 shows the FESEM images of PLA scaffolds with different CNF contents. It is clear that the addition of CNF decreased the pore size, as reported by Zhang and Cui [34], who obtained similar findings. The average pore sizes estimated from the FESEM measurements are listed in Table 1. Figure 1(a)–(e) show that the produced PLA/CNF scaffolds had a highly interconnected pore structure. Moreover, when the CNF content was increased, the overall homogeneity of the scaffold structure was significantly enhanced, leading to a reduction in the pore size. In addition, surface roughness is a crucial factor affecting cell adhesion, growth, and maturation, as mentioned by Cai *et al*. [35]. Therefore, increases in CNF content will greatly enhance the surface roughness of the scaffolds to aid extracellular matrix (ECM) generation.

Based on Figure 1(a) and (b), the surfaces of the PLA_C and PLA/CNF_5 scaffolds were smoother and more uniform. In contrast, a rough and irregular surface was observed on the PLA/CNF-PP_{10}, PLA/CNF-PP_{15}, and PLA/CNF-PP_{20} scaffolds, caused by the dispersion of CNFs. In the pore walls, fibrous structures were visible in the FESEM images (Figure 1d and e). The distributions of the CNFs on the cross-sectional surface of the scaffolds were uniform, illustrating that the biocomposite scaffolds with uniform distribution of CNFs were obtained and attached strongly to the PLA matrix. Image analysis indicated that the average pore sizes were reduced by 134 ± 40.18, 136.68 ± 67.31, 102.98 ± 41.63, 81.48 ± 24.23, and 67.58 ± 18.96 μm for PLA_C, PLA/CNF-PP_5, PLA/CNF-PP_{10}, PLA/CNF-PP_{15}, and PLA/CNF-PP_{20}, respectively. The exact values of the pore size were measured using ImageJ software. As shown in Table 1, although increasing the CNF content reduced the pore size or porosity, this trend continued for CNF concentrations above 15 wt%. As described, the PLA/CNF scaffold with 20 wt% of CNFs had the smallest pores and the lowest porosity among all the scaffolds. As shown in Figure 1(e), the arrangement of the CNF network was denser and, as estimated, led to a decrease in the porosity of PLA/CNF-PP_{20}. This finding could be attributed to the changes in viscosity and conductivity and was influenced by the CNF content, as reported in a previous study [36]. These results illustrate the strong effects of CNF reinforcement on the pore structure of the fabricated scaffolds and their influence on the cell adhesion and proliferation of the PLA/CNF scaffolds.

Large standard deviations were obtained for all scaffolds, with average pore sizes in the range of 67–137 μm. The largest average pore sizes were observed for the pure

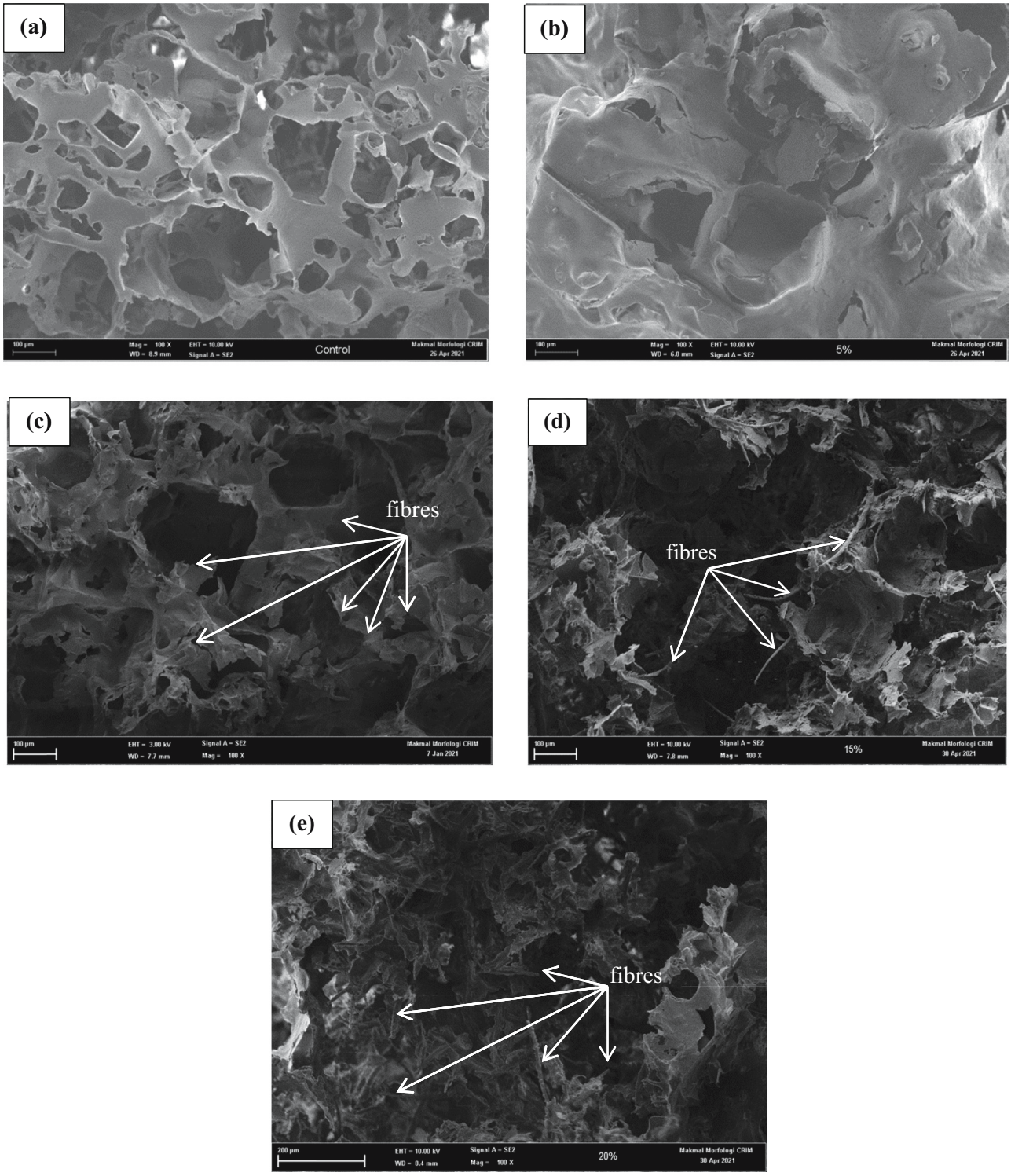

Figure 1: FESEM structure of (a) $PLA_{CONTROL}$, (b) PLA/CNF-PP_5, (c) PLA/CNF-PP_{10}, (d) PLA/CNF-PP_{15}, and (e) PLA/CNF-PP_{20}.

PLA scaffold and scaffold containing minimal CNFs (PLA/CNF-PP_5). When comparing the scaffolds with different CNF contents, PLA/CNF-PP_{15} showed a relatively homogenous surface structure and was highly interconnected. Therefore, due to its average pore size, homogeneity, interconnectivity, and porosity, PLA/CNF-PP_{15} was considered ideal for tissue engineering. Based on the FESEM analysis shown in Figure 1(d), PLA/CNF-PP_{15} had a well-entangled network of CNFs on the pore walls. This fibrous structure and the roughness of the pore wall may enhance cell

fixation and allow for the development of an ECM after implantation. This is attributed to the fact that the surface roughness of the scaffold aids vascularisation, that is, the amount of diffusion to and from the implanted scaffold for nutrient/oxygen supply and the removal of waste products [30–32]. Based on these findings, micropore sizes below 50 µm allow for scaffold vascularisation (removal of waste products and the supply of nutrients for cells), while pore sizes above 100 µm (large pores) support scaffold colonisation by fibroblasts [33–35,37–39].

Figure 2 shows the porosity percentage of the PLA-based biocomposite scaffolds with various CNF contents. Porosity is the percentage of void space, measured by calculating the volume of voids over the total volume. Ethanol was used to prevent the scaffolds' expansion and collapse due to air drying. The calculated porosities are displayed in Table 1, illustrating that all the fabricated scaffolds showed an ideal porosity [36,40]. The percentage of scaffold porosity was enhanced by 85.87, 80.63, 80.98, 81.01, and 76.89% in PLA_C, PLA/CNF-PP_5, PLA/CNF-PP_{10}, PLA/CNF-PP_{15}, and PLA/CNF-PP_{20}, respectively. These results indicate that porosity decreases with an increasing CNF content. These findings are in agreement with the FESEM observations.

Interestingly, PLA/CNF-PP_5, PLA/CNF-PP_{10}, and PLA/CNF-PP_{15} were found to have similar porosities irrespective of the CNF content. When the CNF content increased while maintaining a constant polymer matrix to porogen ratio (1:9), the density tended to increase due to the denser packing of the CNF network and, as predicted, this led to a decrease in porosity [41,42]. This also contributes to the deposition of CNFs on the pore walls, reducing the availability of void areas. Among the scaffolds, those with 20 wt% of CNF (PLA/CNF-PP_{20}) showed the lowest porosity of 76.89%, contributing to the compact arrangement of the CNF network. This also led the scaffold to have a structure with a reduced homogeneity. These results indicate that the reinforcement of CNFs on PLA-based scaffolds plays an important role in controlling the porosity of the scaffolds. On the other hand, researchers have found that a higher porosity may weaken the mechanical performance of the scaffolds, which is not desirable in tissue engineering [21,43,44]. Therefore, cell viability and proliferation can be developed by modifying the pore size, porosity, or both [45].

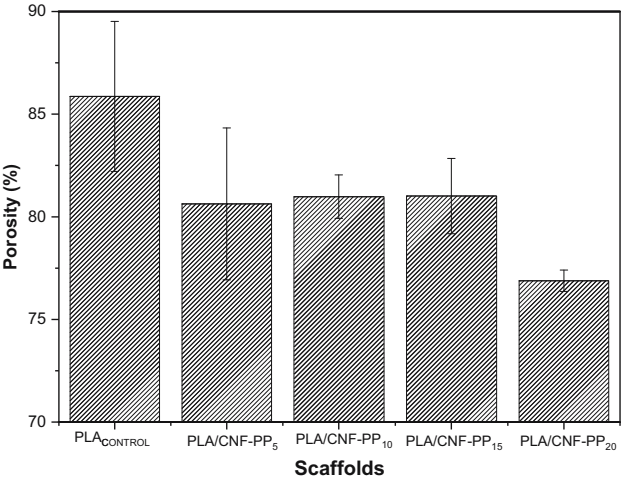

Figure 2: Porosity measurements of PLA scaffolds with different CNF contents.

3.2 XRD analysis

XRD measurements were performed to determine the crystalline structure of the biocomposite scaffolds after reinforcing different CNF contents with a PLA matrix. Figure 3 shows the XRD spectra of the PLA/CNF scaffolds. Generally, the shape of the XRD patterns acquired from the PLA scaffolds with different CNF contents from *Pennisetum purpureum* were similar to those of the pure PLA scaffold, despite the weakening of diffraction peaks in the PLA/CNF scaffolds with an increasing CNF content. The characteristic peaks of CNF from *Pennisetum purpureum* were not observed in the diffraction pattern of the PLA/CNF scaffolds. After the addition of CNF, the intensity of the characteristic peaks was reduced. Broad diffraction with a major semi-crystalline peak was observed at 2θ = 16.8°, while another minor peak was observed at 2θ = 19.3°.

The crystallinity percentage of the PLA/CNF scaffolds was calculated using the XRD diffraction patterns. As shown in Table 2, the crystallinity of the PLA_C, PLA/CNF-PP_5, PLA/CNF-PP_{10}, PLA/CNF-PP_{15}, and PLA/CNF-PP_{20} scaffolds was 65.66, 62.09, 61.48, 61.91, and 61.26%, respectively. These results indicate that an increased CNF content in PLA/CNF scaffolds decreases their crystallinity. The PLA_C scaffold showed the highest degree of crystallinity at 65.66%, where sharper diffraction was demonstrated with an intense peak at 16.8° compared to PLA scaffolds with CNF reinforcements. The difference in crystallinity between scaffolds with varying CNF contents did not differ significantly. The crystallite size was calculated using the Scherrer equation; the crystallite sizes of the PLA_C, PLA/CNF-PP_5, PLA/CNF-PP_{10}, PLA/CNF-PP_{15}, and PLA/CNF-PP_{20} scaffolds were 4.22, 4.04, 3.03, 3.04, and 2.96 nm, respectively. The interplanar spacings of the PLA_C, PLA/CNF-PP_5, PLA/CNF-PP_{10}, PLA/CNF-PP_{15}, and PLA/CNF-PP_{20} scaffolds were 5.30, 5.30, 5.28, 5.29 and 5.31, respectively. Based on the varying contents of

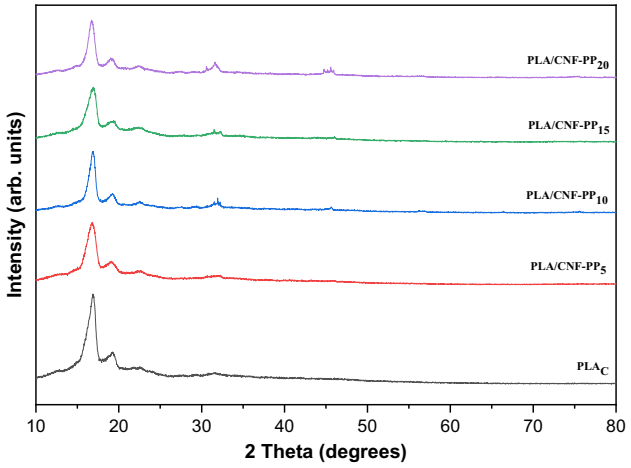

Figure 3: XRD analysis of PLA scaffolds with different CNF contents.

CNF in the PLA/CNF scaffolds, the crystallisation readings showed slight differences in the interplanar spacing. Similarly, Ma *et al.* also studied the XRD of a PLA/hydroxyapatite/graphene oxide nanocomposite, and apart from weakening the diffraction peak of PLA, they also obtained a diffraction pattern similar to that of the nanocomposites [46].

As shown in Figure 3, the degree of crystallinity of the PLA/CNF scaffolds was influenced by two factors: (1) the addition of CNFs and (2) the CNF content distinguishing the interfacial bonding between the polymer matrix and fillers. By varying the CNF content in the PLA/CNF scaffolds, the crystalline structure of the scaffolds could be altered. This may impact the mechanical behaviour and degradability of the fabricated scaffolds. Nevertheless, based on the results and interpretations, it can be concluded that the PLA/CNF scaffolds contain similar diffraction patterns, which may be attributed to the concept that all the scaffolds possess similar microstructures and compositions. This is consistent with the findings from the FTIR spectrum (Figure 4).

3.3 FTIR analysis

IR spectroscopy is commonly used to interpret functional groups and identify intermolecular and intramolecular elements in scaffolds [47]. The most relevant FTIR results of the pure PLA and PLA scaffolds reinforced with various CNF contents from *Pennisetum purpureum* are shown in Figure 4. The weak absorption band at 2,997 cm^{-1} was assigned to the C–H_3 stretching vibration. A band shift related to the CH_3 stretching in the monomer in 2,997–2,923 cm^{-1} was observed in the PLA scaffolds with a varying content of CNF from *Pennisetum purpureum*. These bands, which show a shift in monomer, also displayed a change in peak intensity, indicating the distribution of the polymeric chains. The –C≡C– stretching vibration appeared weak and broadband at 2,160 cm^{-1}. The absorption band corresponding to the C═O stretching vibration found at 1,751 cm^{-1} belonged to the ester group. The band around 1,452 cm^{-1} was related to the C–H_3 bending vibration, whereas C–H bending and C–O stretching vibrations were observed at 1,368 and 1,190 cm^{-1}, respectively. At 1,084 cm^{-1}, a C–C vibration was detected in PLA/CNF scaffolds. The absorption bands observed at 868 and 747 cm^{-1} indicated the presence of aromatic C–H bending. Based on the results, all scaffolds demonstrated identical bands, indicating no change in the chemical structure despite variations in the CNF content. However, differences were observed among the intensities of the stretching bands of the scaffolds. In elaboration, the intensities of the absorption band at 1,751 cm^{-1} of pure PLA were greater than that of PLA scaffolds reinforced with CNF, which can be associated with the overlapping effects of CNF content. In addition, the original strong band of the PLA element at 1,084 cm^{-1} was found to become significantly weaker and broader with an increased CNF content. These results indicate that the main spectrum characteristics of the pure PLA scaffold were very similar to those of the PLA scaffolds reinforced with a varying CNF content from *Pennisetum purpureum*, demonstrating an apparent cross-linking between the PLA (carboxyl group) and CNF (hydroxyl group) of the prepared scaffolds, which is in agreement with the literature [48–53].

3.4 Thermal analysis

The effect of CNF reinforcement on the thermal behaviour of PLA/CNF composite scaffolds was studied using TGA.

Table 2: XRD analysis data of PLA scaffolds with different CNF contents

Sample name	Crystallite size (D, nm)	Interplanar spacing (Å)	Crystallinity (%)
PLA_C	4.22	5.30	65.66
PLA/CNF-PP_5	4.04	5.30	62.09
PLA/CNF-PP_{10}	3.03	5.28	61.48
PLA/CNF-PP_{15}	3.04	5.29	61.91
PLA/CNF-PP_{20}	2.96	5.31	61.26

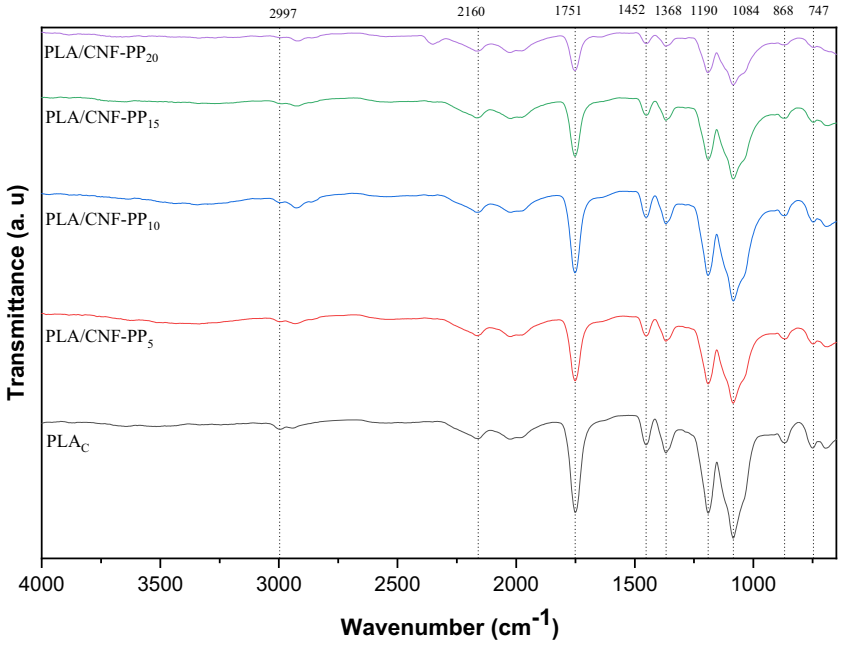

Figure 4: FTIR analysis of PLA scaffolds with different CNF contents.

The TG curves illustrate the thermal stability of the composite scaffolds, while the DTG curves indicate the decomposition temperature of the composite scaffolds. Therefore, the TG and DTG curves as a function of the temperature or time of the PLA/CNF composite scaffolds were collected, as displayed in Figure 5(a)–(e). The thermal parameters, including the initial degradation temperature, degradation temperature at 50% weight loss, final degradation temperature, and weight of char residue, are summarised in Table 3 for all the composite scaffolds.

The initial degradation temperature of the PLA_C, PLA/CNF-PP_5, PLA/CNF-PP_{10}, PLA/CNF-PP_{15}, and PLA/CNF-PP_{20} scaffolds was 324.9, 321.2, 310.0, 305.7, and 299.9°C, respectively. Therefore, it is evident that the values of the scaffolds reinforced with CNF showed a considerable decrease. The initial degradation temperature of the PLA/CNF scaffolds was 25°C lower than that of $PLA_{CONTROL}$. The decrease in the initial degradation temperature of these scaffolds was attributed to the incorporation of CNFs into the PLA matrix, where the polymer chain may be restricted by the dispersion of CNF [45,54–57]. Table 3 shows the degradation temperatures of all scaffolds at 50% of weight loss. In the case of the PLA_C, PLA/CNF-PP_5, PLA/CNF-PP_{10}, PLA/CNF-PP_{15}, and PLA/CNF-PP_{20} scaffolds, these values were 349.9, 346.1, 340.0, 340.7, and 342.5°C, respectively. The degradation temperature decreased slightly as the CNF content increased. The thermal stabilisation of the PLA/CNF scaffolds could be attributed to the dispersion of CNF in the PLA matrix, which influences the interfacial bonding between the PLA matrix and CNF filler.

In addition, the final degradation temperatures of the PLA_C, PLA/CNF-PP_5, PLA/CNF-PP_{10}, PLA/CNF-PP_{15}, and PLA/CNF-PP_{20} scaffolds were 361.4, 355.2, 346.5, 348.2, and 347.9°C, respectively. Thus, the thermal stability of the PLA/CNF scaffolds was significantly reduced by increasing the CNF content. Figure 5(b)–(e) show that the values of the initial and final degradation temperatures of the PLA/CNF scaffolds were lower than that of $PLA_{CONTROL}$. A similar finding was also obtained in the case of silver nanoparticles/cellulose studied by Indira Devi *et al.* [11]. The TG curves of the PLA/CNF scaffolds are illustrated in Figure 5(a)–(e). By analysing the curves, the percentage of char residue weight after the thermal analysis appears to reflect the influence of the CNF reinforcements on the PLA matrix. The PLA_C, PLA/CNF-PP_5, PLA/CNF-PP_{10}, PLA/CNF-PP_{15}, and PLA/CNF-PP_{20} scaffolds had char residue weight percentages of 2.0, 2.7, 3.2, 5.7, and 11.2%, respectively. Thus, the char residue weight of the PLA/CNF scaffolds after TGA analysis was less than 12% of the total weight. However, the char residue weights of the PLA/CNF scaffolds were higher than that of $PLA_{CONTROL}$. This is predictable because PLA is almost completely degraded, while CNF remains in the form of residue even at 800°C. In addition, improvements in char formation may be attributed to the high heat resistance exerted by the CNF reinforcements [58].

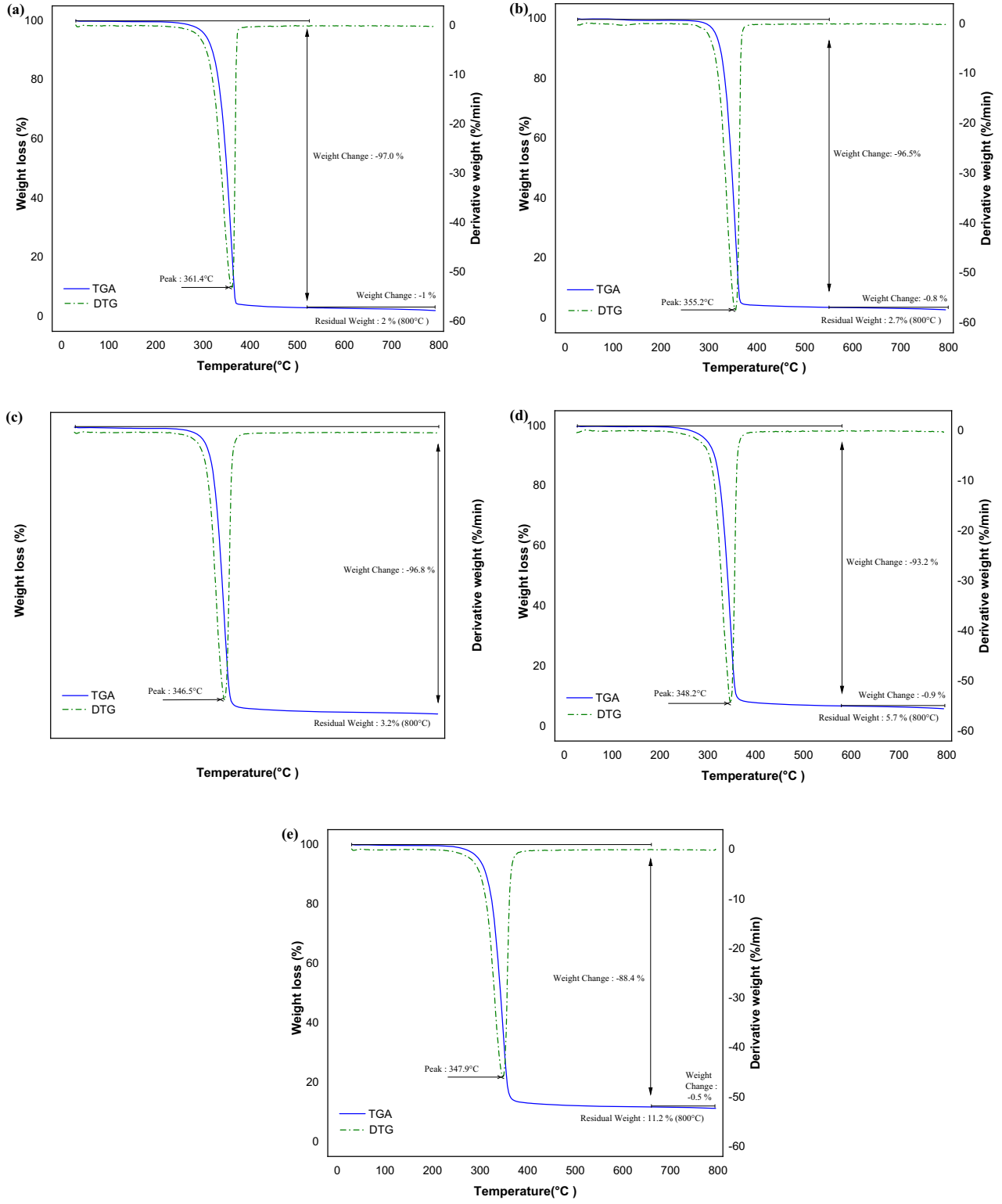

Figure 5: TGA and DTG analysis of (a) $PLA_{CONTROL}$, (b) PLA/CNF-PP_5, (c) PLA/CNF-PP_{10}, (d) PLA/CNF-PP_{15}, and (e) PLA/CNF-PP_{20}.

With the reinforcement of CNF from *Pennisetum purpureum*, the thermal behaviour of the PLA/CNF scaffolds did not change significantly, and the findings for all the scaffolds were similar. As shown in the figures, the TG and DTG curves revealed that all the scaffolds degraded *via* a single-stage weight loss with an approximately

Table 3: TGA results obtained for the PLA_C, PLA/CNF-PP_5, PLA/CNF-PP_{10}, PLA/CNF-PP_{15}, and PLA/CNF-PP_{20} scaffolds

Sample name	Initial degradation temperature (°C)	Degradation at 50% weight loss (°C)	Final degradation temperature (°C)	Char residue weight at 800°C (%)
PLA_C	324.9	349.9	361.4	2.0
PLA/CNF-PP_5	321.2	346.1	355.2	2.7
PLA/CNF-PP_{10}	310.0	340.0	346.5	3.2
PLA/CNF-PP_{15}	305.7	340.7	348.2	5.7
PLA/CNF-PP_{20}	299.9	342.5	347.9	11.2

narrow temperature range, illustrating the uniform solubility of CNF in the PLA matrix. Therefore, the reinforcement of CNF from *Pennisetum purpureum* in the PLA matrix slightly increased the release rate of the scaffolds; hence, the thermal stability of the PLA/CNF scaffolds was reasonably reduced. The results obtained from the thermal analysis showed that the biocomposite scaffolds based on the PLA and CNFs from *Pennisetum purpureum* as reinforcement are in good agreement with the findings for the thermal decomposition of polymer CNF composites [10,17,47].

3.5 Water absorption measurement

The ability of a scaffold to absorb water can be considered an important criterion for evaluating fluid uptake from the surrounding medium [59]. Hence, this measurement plays a crucial role as an indicator of the suitability of a scaffold for tissue engineering. The percentages of water absorption for scaffolds with various CNF contents are shown in Figure 6. The water absorption behaviour of

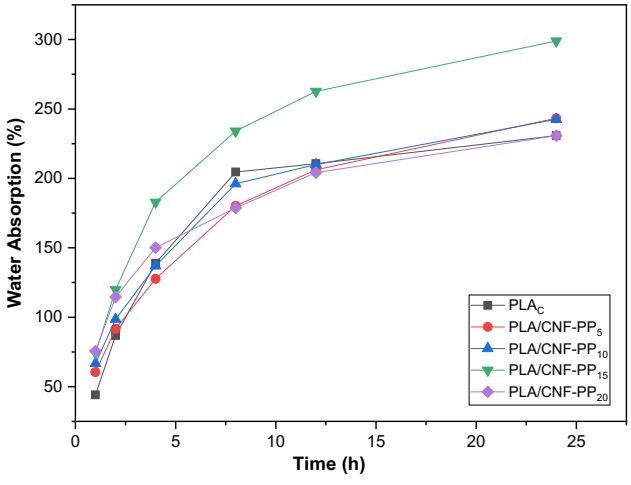

Figure 6: Water absorption measurements of PLA scaffolds with different CNF contents as a function of soaking time.

PLA scaffolds reinforced with CNF from *Pennisetum purpureum* was found to follow non-Fickian in nature [60], whereas the surface area to volume ratio, scaffold size, structure, and the chemistry at the nanoscale control the diffusion and absorption of the scaffolds [8]. For PLA/CNF-PP_5, it was found that by adding up to 5 wt% of CNF, the percentage of water absorption showed an increasing trend compared to that of PLA_C. By further increasing the CNF content, a similar trend was observed for PLA/CNF-PP_{10}, where the percentage of water absorption of PLA/CNF-PP_5 and PLA/CNF-PP_{10} was almost the same. These occurrences occurred because of the hydroxyl group, which acts as a binder between PLA and CNF. In PLA/CNF-PP_{15}, it is evident that by adding 15 wt% of CNF, the water absorption ability of the scaffold showed the most satisfactory improvement. However, at the highest CNF content (20 wt%), the water absorption of the scaffold was lower than that of the scaffolds with CNF. This may be due to the compact arrangement of CNF with the PLA matrix, which influences the porosity and interconnectivity of the PLA matrix with fillers in the scaffold. These findings are supported by the FESEM images and porosity measurements shown in Figures 1(e) and 2. Similarly, Ilyas *et al.* also studied the water absorption of bionanocomposites by mixing sugar palm nanocrystalline cellulose with sugar palm starch using the solution casting method. They mentioned that the high crystallisation of nanocellulose concentration in the nanocomposites might attribute to the decrease in the coefficient of diffusion and equilibrium water uptake of the nanocomposites [61]. Based on these results, CNF from *Pennisetum purpureum* has a good hydrophilic feature. Therefore, it can be concluded that the addition of CNF to scaffolds increases the ability of the scaffolds to absorb water significantly, as shown in Figure 6. Even though the PLA matrix is not a useful candidate for cell attachment and proliferation, the reinforcement of CNF not only enhances the mechanical strength and structural properties but also help to improve the hydrophilicity of the scaffolds, which contributes to a friendly environment for cell culture.

Table 4: Mechanical properties of PLA scaffolds with different CNF contents

Samples	Compression strength (MPa)	Increase (%)	Compression modulus (MPa)	Increase (%)
$PLA_{CONTROL}$	2.37 ± 0.65	0	1.95 ± 0.67	0
PLA/CNF-PP_5	2.96 ± 1.17	25	2.79 ± 1.10	43
PLA/CNF-PP_{10}	4.13 ± 1.24	74	4.20 ± 1.41	115
PLA/CNF-PP_{15}	6.66 ± 1.99	181	6.04 ± 1.69	210
PLA/CNF-PP_{20}	3.26 ± 1.27	38	3.16 ± 1.06	62

3.6 Mechanical properties

The influence of the addition of CNFs from *Pennisetum purpureum* on the mechanical performance of the fabricated scaffolds was investigated through compressive tests. According to reviews, an ideal scaffold for tissue regeneration should steadily transfer stress to the newly formed tissue during cell proliferation; thus, an appropriate material and fabrication technique are crucial for tuning both the microstructure and mechanical properties [62]. Table 4 presents the mechanical properties of pure PLA and PLA scaffolds reinforced with 5, 10, 15, and 20 wt% of CNF from *Pennisetum purpureum*. The compressive strength and modulus were approximately 70% of the initial height of the samples. The PLA_C scaffold had an average compressive strength of 2.37 ± 0.65 MPa and a compressive modulus of 1.95 ± 0.67 MPa. On the other hand, the PLA/CNF-PP_5 and PLA/CNF-PP_{10} scaffolds had an average compressive strength of 2.96 ± 1.17 and 4.13 ± 1.24 MPa, and a compressive modulus of 2.79 ± 1.10 and 4.20 ± 1.41 MPa, respectively. Thus, the compressive strength increased by 25 and 74% from PLA_C to PLA/CNF-PP_5 and PLA/CNF-PP_{10} scaffolds, while the compressive modulus increased by 43 and 115% from PLA_C to PLA/CNF-PP_5 and PLA/CNF-PP_{10} scaffolds, respectively. Meanwhile, the compressive strength of the PLA/CNF-PP_{15} and PLA/CNF-PP_{20} scaffolds were 6.66 ± 1.99 and 3.26 ± 1.27 MPa, while the compressive modulus of the PLA/CNF-PP_{15} and PLA/CNF-PP_{20} scaffolds were 6.04 ± 1.69 and 3.16 ± 1.06 MPa, respectively. Thus, the compressive strength increased by 181 and 38% from the PLA_C to PLA/CNF-PP_{15} and PLA/CNF-PP_{20} scaffolds, whereas the compressive modulus increased by 210 and 62% from the PLA_C to PLA/CNF-PP_{15} and PLA/CNF-PP_{20} scaffolds, respectively.

As expected, the reinforcement of CNFs from *Pennisetum purpureum* improved both the compressive strength and modulus of the fabricated scaffolds, which clearly illustrates the specific advantage of PLA/CNF composites in the preparation of scaffolds for tissue engineering. PLA/CNF-PP_{15} displayed a significantly higher compressive strength and modulus than scaffolds with different CNF compositions. On the other hand, the enhancement of the compression properties of PLA/CNF scaffolds may be associated with the dispersion of CNFs. The rigid network of hydrogen bonding between PLA and CNFs resulted in an excellent load transfer from the polymer matrix to the CNFs. However, the increment of CNFs from 15 to 20 wt% led to a noticeable decrease in the

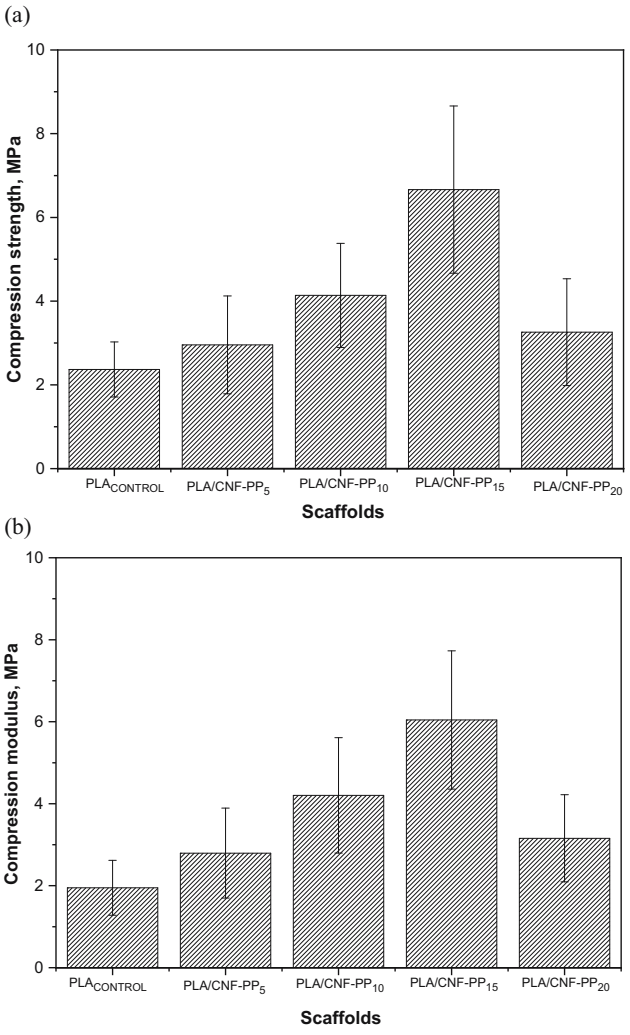

Figure 7: (a) Compression strength and (b) compression modulus of PLA scaffolds with different CNF contents.

compression properties, as shown in Table 4. As shown in Figure 7(a) and (b), PLA/CNF-PP_{20} showed a marked decrease in compressive strength and compressive modulus, approximately 38 and 62%, respectively, compared to PLA/CNF-PP_{10} and PLA/CNF-PP_{15}. Thus, despite the fact that the reinforcement of CNFs improves their mechanical properties, CNFs tend to agglomerate at higher contents and may cause poor performance [63]. In addition, a weak microstructure and heterogeneous porosity were subjected to higher CNF content, as proven by the PLA/CNF-PP_{20} scaffold. Nasri-Nasrabadi *et al.* [64] and Shuai *et al.* [65] investigated the influence of the addition of CNFs to starch and nano-hydroxyapatite to poly(lactide-co-glycolide). In both studies, the reinforcement of fillers showed a marked increase in the compression properties of the composite scaffolds. However, when the filler content was increased over 15–30 wt%, the compressive properties decreased.

The compressive strength of trabecular bone differs depending on bone density (2–10 MPa) [66,67]. As previously mentioned, CNFs from *Pennisetum purpureum* were found to improve the compression properties of the PLA composite scaffolds; values significantly similar to those of trabecular bone were obtained for all the scaffolds. Soft tissue substitute composites must have mechanical properties identical to those of the host tissue. When the difference between compression modulus is large, a heterogeneous distribution of load will be created, leading to the failure of the implant [68]. However, this study demonstrated that the combination of PLA and CNFs from *Pennisetum purpureum* allowed for the fabrication of scaffolds with higher strength, modulus, and rigidity.

4 Conclusion

In this study, PLA scaffolds reinforced with CNFs from *Pennisetum purpureum* with interconnected pores were developed using solvent casting and particulate leaching techniques. The morphology of the scaffolds was found to vary depending on the content of the CNFs. In addition, FESEM images showed that the scaffolds had good porosity and interconnected pores, a high surface area, and good fluid retention capacity, which in turn encouraged cell attachment and proliferation. The XRD and FTIR spectra showed no significant changes in the PLA matrix structure by reinforcing the CNFs. The decomposition temperature of the composite scaffolds was lower than that of the PLA control due to interfacial bonding between the PLA matrix and the CNF fillers. The water absorption of the scaffold was enhanced by the inclusion of fillers up to 15 wt%, while PLA with 20 wt% fillers showed a decreasing trend due to the compact arrangement of CNFs, as illustrated in the FESEM images. The tendency of CNFs to agglomerate plays a crucial criterion in improving the hydrophilicity of the composite scaffolds. TGA analysis indicated a considerable decrease as the CNF content increased. The reinforcement of 15 wt% CNFs enhanced the compressive strength by approximately 181% and compressive modulus by 210%. However, a further increase in the CNF content to 20 wt% (PLA/CNF-PP_{20}) led to a significant decrease in the compressive strength and modulus. The compressive strength and modulus of the scaffolds were found to be within the range of properties shown for trabecular bone. These results suggest that PLA/CNF scaffolds with a maximum of 15 wt% of CNF from *Pennisetum purpureum* have the potential for use in tissue engineering as a biomaterial.

Acknowledgements: The authors gratefully acknowledge i-CRiM, Universiti Kebangsaan Malaysia, for providing the analytical services.

Funding information: The Ministry of Higher Education Malaysia financed this research through the Fundamental Research Grant Scheme (FRGS/1/2019/TK05/UNIMAP/03/5).

Author contributions: All authors have accepted responsibility for the entire content of this manuscript and approved its submission.

Conflict of interest: The authors state no conflict of interest.

References

[1] Pei B, Wang W, Fan Y, Wang X, Watari F, Li X. Fiber-reinforced scaffolds in soft tissue engineering. Regen Biomater. 2017;4(4):257–68.
[2] Yuksel E, Choo J, Wettergreen M, Liebschner M. Challenges in soft tissue engineering. Semin Plast Surg. 2005;19(3):261–70.
[3] Chakrabarty A, Teramoto Y. Recent advances in nanocellulose composites with polymers: a guide for choosing partners and how to incorporate them. Polym (Basel). 2018;10(5):517.
[4] Asim M. Nanocellulose: preparation methods and applications. In: Cellulose-reinforced nanofibre composites. Sawston, UK: Woodhead Publishing; 2017. p. 261–76.
[5] Kargarzadeh H, Ioelovich M, Ahmad I, Thomas S, Dufresne A. Methods for extraction of nanocellulose from various sources. Handbook of Nanocellulose and Cellulose Nanocomposites. Weinheim, Germany: Wiley-VCH; 2017. p. 1–49.

[6] Shak KPY, Pang YL, Mah SK. Nanocellulose: recent advances and its prospects in environmental remediation. Beilstein J Nanotechnol. 2018;9(1):2479–98.
[7] Kian LK, Saba N, Jawaid M, Sultan MTH. A review on processing techniques of bast fibers nanocellulose and its polylactic acid (PLA) nanocomposites. Int J Biol Macromol. 2019;121:1314–28.
[8] Hickey RJ, Pelling AE. Cellulose biomaterials for tissue engineering. Front Bioeng Biotechnol. March 2019;7:1–15.
[9] Reddy KO, Maheswari CU, Shukla M, Rajulu AV. Chemical composition and structural characterisation of Napier grass fibers. Mater Lett. 2012;67(1):35–8.
[10] Haameem MJA, Majid MSA, Afendi M, Marzuki HFA, Fahmi I, Gibson AG. Mechanical properties of Napier grass fibre/polyester composites. Compos Struct. 2016;136:1–10.
[11] Indira Devi MP, Nallamuthu N, Rajini N, Varada Rajulu A, Hari Ram N, Siengchin S. Cellulose hybrid nanocomposites using Napier grass fibers with in situ generated silver nanoparticles as fillers for antibacterial applications. Int J Biol Macromol. 2018;118:99–106.
[12] Ridzuan MJM, Abdul Majid MS, Afendi M, Aqmariah Kanafiah SN, Zahri JM, Gibson AG. Characterisation of natural cellulosic fibre from Pennisetum purpureum stem as potential reinforcement of polymer composites. Mater Des. Jan. 2016;89:839–47.
[13] De Araújo Morandim-Giannetti A, Albuquerque TS, De Carvalho RKC, Araújo RMS, Magnabosco R. Study of 'Napier grass' delignification for production of cellulosic derivatives. Carbohydr Polym. 2013;92(1):849–55.
[14] Bacakova L, Pajorova J, Bacakova M, Skogberg A, Kallio P, Kolarova K, et al. Versatile application of nanocellulose: from industry to skin tissue engineering and wound healing. Nanomaterials. 2019;9(2):164.
[15] Jorfi M, Foster EJ. Recent advances in nanocellulose for biomedical applications. J Appl Polym Sci. 2015;132(14):1–19.
[16] Radakisnin R, Majid MSA, Jamir MRM, Jawaid M, Sultan MTH, Tahir MFM. Structural, morphological and thermal properties of cellulose nanofibers from Napier fiber (Pennisetum purpureum). Mater (Basel). 2020;13(18):4125.
[17] Jian W, Hui D, Lau D. Nanoengineering in biomedicine: current development and future perspectives. Nanotechnol Rev. 2020;9(1):700–15.
[18] Madhavan Nampoothiri K, Nair NR, John RP. An overview of the recent developments in polylactide (PLA) research. Bioresour Technol. 2010;101:8493–501.
[19] Dai W, Yang Y, Yang Y, Liu W. Material advancement in tissue-engineered nerve conduit. Nanotechnol Rev. 2021;10(1):488–503.
[20] Oksman K, Skrifvars M, Selin J-F. Natural fibres as reinforcement in polylactic acid (PLA) composites. Compos Sci Technol. 2003;63(9):1317–24.
[21] Xiao L, Wang B, Yang G, Gauthier M. Poly(Lactic Acid)-based biomaterials: synthesis, modification and applications. Biomed Sci Eng Technol. 2006;11:247–82.
[22] Lopes MS, Jardini AL, Filho RM. Poly (lactic acid) production for tissue engineering applications. Procedia Eng. 2012;42:1402–13.
[23] Grémare A, Guduric V, Bareille R, Heroguez V, Latour S, L'heureux N, et al. Characterization of printed PLA scaffolds for bone tissue engineering. J Biomed Mater Res A. 2018;106(4):887–94.
[24] Donate R, Monzón M, Alemán-Domínguez ME, Ortega Z. Enzymatic degradation study of PLA-based composite scaffolds. Rev Adv Mater Sci. 2020;59(1):170–5.
[25] Navarro M. 3D printed PLA-based scaffolds. Organogenesis. 2013;9(4):239–44.
[26] Dave HK, Rajpurohit SR, Patadiya NH, Dave SJ, Sharma KS, Thambad SS, et al. Compressive strength of PLA based scaffolds: effect of layer height, infill density and print speed. Int J Mod Manuf Technol. 2019;11(1):21–7.
[27] Peng Z, Tang P, Zhao L, Wu L, Xu X, Lei H, et al. Advances in biomaterials for adipose tissue reconstruction in plastic surgery. Nanotechnol Rev. 2020;9(1):385–95.
[28] Chanda S, Bajwa DS. A review of current physical techniques for dispersion of cellulose nanomaterials in polymer matrices. Rev Adv Mater Sci. 2021;60(1):325–41.
[29] Massai D, Pennella F, Gentile P, Gallo D, Ciardelli G, Bignardi C, et al. Image-based three-dimensional analysis to characterise the texture of porous scaffolds. Biomed Res Int. 2014;2014:161437.
[30] Tairov EA. Method of measuring void fraction in a channel with porous media. Thermophys Aeromechanics. 2020;27(2):313–6.
[31] Choudhury M, Mohanty S, Nayak S. Effect of different solvents in solvent casting of porous PLA scaffolds – in biomedical and tissue engineering applications. J Tissue Sci Eng. 2014;6(1):1–7.
[32] ASTM D695-96, Standard Test Method for Compressive Properies of Rigid Plastics, ASTM International, West Conshohocken, PA, 2021.
[33] Doulabi AH, Mequanint K, Mohammadi H. Blends and nanocomposite biomaterials for articular cartilage tissue engineering. Mater (Basel). 2014;7(7):5327–55.
[34] Zhang Z, Cui H. Biodegradability and biocompatibility study of poly(chitosan-g-lactic acid) scaffolds. Molecules. 2012;17:3243–58.
[35] Cai S, Wu C, Yang W, Liang W, Yu H, Liu L. Recent advance in surface modification for regulating cell adhesion and behaviors. Nanotechnol Rev. 2020;9(1):971–89.
[36] Naseri N, Lenart G, Kristiina O. 3-Dimensional porous nanocomposite scaffolds based on cellulose nanofibers for cartilage tissue engineering: tailoring of porosity and mechanical performance. R Soc Chem. 2016;6:5999–6007.
[37] Hagen R. Basics of PLA. Bioplastics Mag. 2005;4:38–40.
[38] Chung HJ, Park TG. Surface engineered and drug releasing prefabricated scaffolds for tissue engineering. Adv Drug Deliv Rev. 2007;59:249–62.
[39] Bartis D, Pongrácz J. Three dimensional tissue cultures and tissue engineering. In: Teaching Materials: Medical Biotechnology Master's Program. Debrecen: University of Pécs; 2011. p. 15.
[40] Loh QL, Choong C. Three-dimensional scaffolds for tissue engineering applications: role of porosity and pore size. Tissue Eng B Rev. 2013;19(6):485–502.
[41] Bartoš M, Suchý T, Foltán R. Note on the use of different approaches to determine the pore sizes of tissue engineering scaffolds: what do we measure? Biomed Eng Online. 2018;17(1):1–15.

[42] Chen G, Ushida T, Tateishi T. Development of biodegradable porous scaffolds for tissue engineering. Mater Sci Eng C. 2001;17(1):63–9.
[43] Ma PX. Scaffolds for tissue fabrication. Mater Today. 2004;7:30–40.
[44] Razak SIA, Sharif NFA, Rahman WAA. Biodegradable polymers and their bone applications: a review. Int J Basic Appl Sci. 2012;12:31–49.
[45] Lien SM, Ko LY, Huang TJ. Effect of pore size on ECM secretion and cell growth in gelatin scaffold for articular cartilage tissue engineering. Acta Biomater. 2009;5(2):670–9.
[46] Ma H, Su W, Tai Z, Sun D, Yan X, Liu B, et al. Preparation and cytocompatibility of polylactic acid/hydroxyapatite/graphene oxide nanocomposite fibrous membrane. Chin Sci Bull. 2012;57(23):3051–8.
[47] Niu X, Feng Q, Wang M, Guo X, Zheng Q. In vitro degradation and release behavior of porous poly(lactic acid) scaffolds containing chitosan microspheres as a carrier for BMP-2-derived synthetic peptide. Polym Degrad Stab. 2009;94(2):176–82.
[48] Tang D, Tare RS, Yang LY, Williams DF, Ou KL, Oreffo ROC. Biofabrication of bone tissue: approaches, challenges and translation for bone regeneration. Biomaterials. 01-Mar-2016;83:363–82.
[49] Loh QL, Choong C. Three-dimensional scaffolds for tissue engineering applications: Role of porosity and pore size. Tissue Eng B Rev. 2013;19(6):485–502.
[50] Sehaqui H, Zhou Q, Berglund LA. High-porosity aerogels of high specific surface area prepared from nanofibrillated cellulose (NFC). Compos Sci Technol. Sep. 2011;71(13):1593–9.
[51] Sehaqui H, Salajková M, Zhou Q, Berglund LA. Mechanical performance tailoring of tough ultra-high porosity foams prepared from cellulose i nanofiber suspensions. Soft Matter. Apr. 2010;6(8):1824–32.
[52] Ploypetchara N, Suppakul P, Atong D, Pechyen C. Blend of polypropylene/poly(lactic acid) for medical packaging application: physicochemical, thermal, mechanical, and barrier properties. Energy Procedia. 2014;56:201–10.
[53] Bulota M, Budtova T. PLA/algae composites: Morphology and mechanical properties. Compos Part A Appl Sci Manuf. 2015;73:109–15.
[54] Shokrolahi F, Mirzadeh H, Yeganeh H, Daliri M. Fabrication of poly(urethane urea)-based scaffolds for bone tissue engineering by a combined strategy of using compression moulding and particulate leaching methods. Iran Polym J. Jan. 2011;20(8):645–58.
[55] Chen G, Ushida T, Tateishi T. Scaffold design for tissue engineering. Macromol Biosci. 2002;2(2):67–77. Wiley Online Library. [Online]. Available: https://onlinelibrary.wiley.com/doi/abs/10.1002/1616-5195%2820020201%292%3A2%3C67%3A%3AAID-MABI67%3E3.0.CO%3B2-F [Accessed: 10-Jun-2021].
[56] Lee SH, Teramoto Y, Endo T. Cellulose nanofiber-reinforced polycaprolactone/polypropylene hybrid nanocomposite. Compos Part A Appl Sci Manuf. Feb. 2011;42(2):151–6.
[57] Xiong R, Hameed N, Guo Q. Cellulose/polycaprolactone blends regenerated from ionic liquid 1-butyl-3-methylimidazolium chloride. Carbohydr Polym. Sep. 2012;90(1):575–82.
[58] Cheung HY, Lau KT, Tao XM, Hui D. A potential material for tissue engineering: Silkworm silk/PLA biocomposite. Compos Part B Eng. 2008;39:1026–33.
[59] Tohamy KM, Mabrouk M, Soliman IE, Beherei HH, Aboelnasr MA. Novel alginate/hydroxyethyl cellulose/hydroxyapatite composite scaffold for bone regeneration: In vitro cell viability and proliferation of human mesenchymal stem cells. Int J Biol Macromol. January 2018;112:448–60.
[60] Maslinda AB, Abdul Majid MS, Ridzuan MJM, Afendi M, Gibson AG. Effect of water absorption on the mechanical properties of hybrid interwoven cellulosic-cellulosic fibre reinforced epoxy composites. Compos Struct. 2017;167:227–37.
[61] Ilyas RA, Sapuan SM, Ishak MR, Zainudin ES. Development and characterisation of sugar palm nanocrystalline cellulose-reinforced sugar palm starch bionanocomposites. Carbohydr Polym. August 2018;202:186–202.
[62] Raia NR, McGill M, Marcet T, Vidal Yucha SE, Kaplan DL. Soft tissue engineering. Biomaterials Science. Amsterdam, Netherlands: Elsevier; 2020. p. 1399–414.
[63] Kaushik A, Singh M, Verma G. Green nanocomposites based on thermoplastic starch and steam exploded cellulose nanofibrils from wheat straw. Carbohydr Polym. 2010;82(2):337–45.
[64] Nasri-Nasrabadi B, Mehrasa M, Rafienia M, Bonakdar S, Behzad T, Gavanji S. Porous starch/cellulose nanofibers composite prepared by salt leaching technique for tissue engineering. Carbohydr Polym. Aug. 2014;108(1):232–8.
[65] Shuai C, Yang B, Peng S, Li Z. Development of composite porous scaffolds based on poly(lactide-co- glycolide)/nanohydroxyapatite via selective laser sintering. Int J Adv Manuf Technol. Oct. 2013;69(1–4):51–7.
[66] Revati R, Abdul Majid MS, Ridzuan MJM, Normahira M, Mohd Nasir NF, Rahman Y MN, et al. Mechanical, thermal and morphological characterisation of 3D porous Pennisetum purpureum/PLA biocomposites scaffold. Mater Sci Eng C. 2017;75:752–9.
[67] Sheng L, Jiang R, Zhu Y, Ji Y. Electrospun cellulose nanocrystals/polycaprolactone nanocomposite fiber mats. J Macromol Sci Part B Phys. May 2014;53(5):820–8.
[68] Weaver JCJK. Cancellous bone: Its strength and changes with aging and an evaluation of some methods for measuring its mineral content. J Bone Jt Surg. 1966;48A:289–9.